

Non-coherent and Differentially Coherent Code Acquisition in MIMO Assisted DS-CDMA Multi-path Downlink Scenarios

SeungHwan Won, *Student Member, IEEE*, and Lajos Hanzo, *Fellow, IEEE*

Abstract—In this contribution we investigate both Differentially Coherent (DC) and Non-Coherent (NC) code acquisition schemes in the Multiple Input Multiple Output (MIMO)-aided Direct Sequence-Code Division Multiple Access (DS-CDMA) downlink, when communicating over uncorrelated Rayleigh channels. It is demonstrated that the employment of multiple transmit antennas has a detrimental impact on the achievable diversity gain at typical operational Signal-to-Interference plus Noise Ratios (SINR), as the number of transmit antennas is increased, regardless whether single-path or multi-path scenarios are considered. Our findings suggest that increasing the number of transmit antennas in a MIMO-aided CDMA system results in increasing the Mean Acquisition Time (MAT) by as much as an order of magnitude, when the SINR per chip value is relatively low. The main reasons for the performance trends are plausible, since we have to reduce each individual MIMO element's signal power for maintaining the same total power as in a single-antenna system and this will be further justified by information theoretic considerations in the NC MIMO-aided scenarios considered.

Index Terms—Differentially coherent acquisition, non-coherent acquisition, DS-CDMA, serial search, transmit/receive diversity.

I. INTRODUCTION

THE application of multiple antennas in the DownLink (DL) of wireless systems constitutes an attractive technique of reducing the detrimental effects of time-variant multi-path fading environments [1]. In CDMA systems the mobile station's receiver must be capable of accurately aligning the timing of the locally generated PseudoNoise (PN) code with that of the received multi-user signals containing the desired user's PN sequence. Substantial research efforts have been devoted to the design of code acquisition techniques [2],[3],[4]. Although most of the results have been derived for single-input single-output systems, some results concerning multi-path scenarios have also been disseminated in the literature [5],[6]. Hence, apart from [7],[8] there is a paucity of code acquisition techniques designed for transmit diversity-aided systems. In the light of this, representing the fundamental characteristics of code acquisition schemes assisted by multiple transmit/receive antennas in the context of Differentially Coherent (DC) code acquisition schemes is the objective

Manuscript received October 24, 2005; revised July 12, 2006, January 11, 2007, and January 15, 2008; accepted March 13, 2008. The associate editor coordinating the review of this paper and approving it for publication was M. Saquib.

The authors are with the of ECS, Univ. of Southampton, SO17 1BJ, UK (e-mail: lh@ecs.soton.ac.uk).

Digital Object Identifier 10.1109/TWC.2008.05847.

of the present contribution. Similarly to the Non-Coherent (NC) code acquisition schemes described in [3],[4], DC code acquisition [9] also dispenses with any prior information on the carrier phase. An additional benefit of employing a DC code acquisition scheme is that it is capable of providing a better performance than using a NC one [4],[9],[10]. Here we adopted the Full-Period Correlation (FPC) based scheme of [9],[10] for analysing the characteristics of serial search-aided DC code acquisition in the Multiple Input Multiple Output (MIMO)-aided DS-CDMA DL. Furthermore, in the verification mode of the DC scheme described in [11], the characteristics of the MIMO-aided code acquisition schemes were also analysed. Again, the novel contribution of this treatise is that we analytically characterise both serial search based DC and NC code acquisition schemes designed for MIMO-aided systems, since no similar studies are available in the literature. More explicitly, we quantify both the correct detection probability as well as the false alarm probability as a function of the number of transmit/receive antennas and the SINR per chip, E_c/I_0 . Additionally, we characterise the MAT performance, also parameterised by both the E_c/I_0 values and the number of transmit/receive antennas in both single-path and multi-path scenarios.

This paper is organised as follows. The system investigated is introduced in Section II, while Section III describes the correct detection and false alarm probability analysis of both DC and NC code acquisition schemes in the context of uncorrelated Rayleigh channels, followed by the interpretation of MAT expressions. In Section IV, our numerical MAT results are discussed and our conclusions are offered in Section V.

II. SYSTEM DESCRIPTION

We assume that a finite-length tapped delay line channel model generates the L Rayleigh-faded multi-path signals, each arriving with a time delay τ_l having a tap spacing of one chip-duration [5],[12], where $l = 1, \dots, L$ is the number of multi-path components. It is also assumed that the Rayleigh fading is sufficiently slow for the faded envelope to remain constant over τ_D chip intervals, but fast enough so that τ_D consecutive chip segments may be considered essentially independently faded, as in [2],[13],[14], where τ_D is the coherent integration interval used. Furthermore, the Neyman-Pearson criterion [2],[15] is adopted, which leads to a Constant False-Alarm Rate (CFAR). This is because as a benefit of normalising the received signal by the background noise variance estimate, the

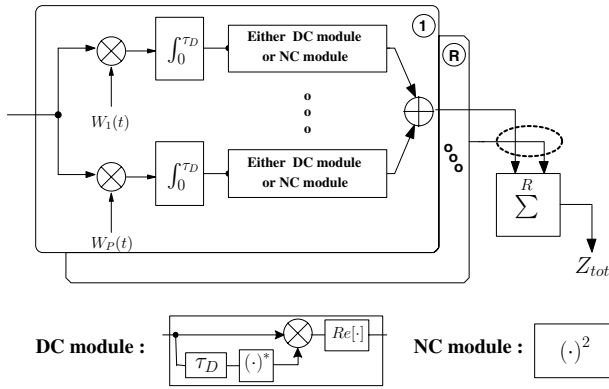


Fig. 1. Receiver structure of both DC and NC code acquisition using R receive antennas. In the context of the search mode constituting the SDSS scheme using the threshold θ_1 only NC detection is possible, while in the verification mode employing the threshold θ_2 both NC and DC acquisition is possible.

fading channel's attenuation no longer affects the outcome of the hypothesis test, regardless whether the desired signal is present or absent. The resultant scenario and the related test becomes reminiscent of an Additive White Gaussian Noise (AWGN) scenario. Consequently, in line with the findings of [2],[15], the mobile channel only affects the correct detection probability.

The received signal of the MIMO-aided DS-CDMA DL over the multi-path Rayleigh fading channel considered may be expressed as [10]

$$r(t) = \sum_{l=1}^L \sum_{m=1}^P \sum_{n=1}^R [\alpha_{(l,m,n)} \sqrt{\frac{E_c}{PT_c}} C(t + dT_c + \tau_l) \cdot w_m(t + dT_c + \tau_l) \exp(2\pi f t + \phi_{(l,m,n)}) + I_{k(l,m,n)}(t)], \quad (1)$$

where P is the number of transmit antennas, R is the number of receive antennas, $\alpha_{(l,m,n)}$ represents the complex-valued envelope of the $(l, m, n)^{th}$ signal path obeying a Rayleigh magnitude distribution and a uniform phase distribution, E_c denotes the pilot signal energy per PN code chip, $C(t)$ is a common PN sequence having a cell-specific code-phase offset, d is the code phase offset with respect to the phase of the local code, T_c is the chip duration, $w_m(t)$ identifies the specific Walsh code assigned to the m^{th} transmit antenna, f is the carrier frequency and finally, ϕ is the carrier phase of a specific user's modulator. Furthermore, $I_{k(l,m,n)}(t)$ is the complex-valued AWGN having a double-sided power spectral density of I_0 at the $(l, m, n)^{th}$ path. Here the total allocated power is equally shared by the P transmit antennas. Fig.1 portrays both the DC and the NC receiver's schematic designed for our code acquisition scheme using transmit/receive antennas, where the timing hypothesis test is carried out for binary spreading. The NC module generates its decision variable by accumulating $P \cdot R$ number of independently faded signals observed over a given time interval. In the DC scheme of Fig.1, instead of squaring the summed energy as suggested by the procedures outlined in [2], the channel's output samples accumulated over a full spreading code period are multiplied by the conjugate of the N -chip-delayed samples, where N is represented by $N = \tau_D/T_c$ [9],[10].

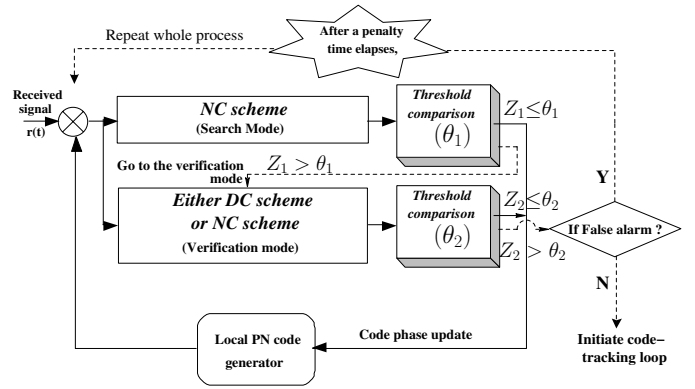


Fig. 2. Receiver flowchart of our DDSS code acquisition scheme, where θ_1 and θ_2 represent the acquisition thresholds of the search and verification modes, respectively. The search mode constitutes the SDSS and consecutive search and verification modes represent the DDSS.

When analysing the MAT performance of the Single Dwell Serial Search (SDSS) technique [2], where the NC receiver structure of Fig.1 is used in the search mode constituting the SDSS scheme seen at the top of Fig.2¹, the decision statistics, Z_{tot} generated by the NC module of Fig.1 are compared to the threshold θ_1 , which is optimised for a specific E_c/I_0 value². This completes the single-step search-mode of the SDSS scheme. By contrast, the Double Dwell Serial Search (DDSS) technique [16] of Fig.2 invokes a two-step process. More explicitly, once the desired user's tentative code phase was found in the search mode of the DDSS scheme of Fig.2, the verification mode is activated. The verification mode may use either the DC or the NC modules of Fig.1, in order to confirm that the correct code-phase is indeed the one identified in the search mode. On the other hand, in the search mode, only the NC scheme can be used, as portrayed in Fig.2. The DC scheme is excluded from the search mode, because it requires further processing carried out within the DC module of Fig.1 and hence the complexity may be minimised by limiting the employment of the DC scheme to the verification mode. More explicitly, the NC scheme is employed in two consecutive decision processes, namely first in finding and then confirming the correct code phase in order to improve the reliability of SDSS, which results in the DDSS acquisition scheme of Fig.2, where θ_1 and θ_2 represent the acquisition thresholds of the search and verification mode, respectively. Furthermore, Z_1 and Z_2 denote the decision variables of the search and verification mode, respectively. In Fig.2 Z_1 is compared to θ_1 and if it exceeds the threshold, Z_2 generated by either DC or NC module is compared to θ_2 . If successful code acquisition is declared, then the code tracking loop is enabled. Otherwise, the acquisition system reverts back to the search-stage, until the correct code and its phase are found. In our forthcoming analysis, four code acquisition arrangements are considered. Specifically, SDSS employing both DC and NC schemes as

¹The term 'update' indicates that the acquisition scheme adjusts or updates the particular code-phase assumed during the current hypothesis test in its efforts to find the best possible alignment of the received and locally stored code [17], given the particular search step-size used.

²The specific value of E_c/I_0 depends on the operating environment.

well as DDSS exploiting both DC and NC arrangements are invoked in the verification mode. Further details on the related DDSS system can be found in [11],[16].

III. ANALYSIS OF DIFFERENTIALLY COHERENT AND NON-COHERENT CODE ACQUISITION

A. Correct Detection and False Alarm Probabilities of the Differentially Coherent Code Acquisition Scheme

A decision variable is generated by accumulating $P \cdot R$ number of independently faded received signals observed over a time interval for improving the correct detection probability in the mobile channel imposing both fading and poor SINR conditions. Here we omitted formulating the final decision variable, which is readily derived from the procedures proposed in [10] in the context of the DC receiver structure of Fig.1. The final DC decision variable of the l^{th} path may be written as [10]

$$Z_{k(l)}^{DC} = \sum_{m=1}^P \sum_{n=1}^R \left[\left(\sqrt{\frac{4E_c}{NI_0P}} \cdot S_{k(l,m,n)} + W_{1,k(l,m,n)} \right)^2 + W_{3,k(l,m,n)}^2 - \sum_{m=1}^P \sum_{n=1}^R \left[W_{2,k(l,m,n)}^2 + W_{4,k(l,m,n)}^2 \right] \right], \quad (2)$$

where k denotes the k^{th} chip's sampling instant and $S_{k(l,m,n)}$ represents a deterministic value, which depends on whether a signal is present or absent [10]. Furthermore, the definition of $W_{1,k(l,m,n)}$, $W_{2,k(l,m,n)}$, $W_{3,k(l,m,n)}$ and $W_{4,k(l,m,n)}$ is the same as in [10], which are mutually independent Gaussian random variables having zero means and unit variances [10]. Let us now introduce a shorthand for the first and second terms of Eq(2) as follows:

$$X_{k(l)} = \sum_{m=1}^P \sum_{n=1}^R \left[\left(\sqrt{\frac{4E_c}{NI_0P}} \cdot S_{k(l,m,n)} + W_{1,k(l,m,n)} \right)^2 + W_{3,k(l,m,n)}^2 \right] \quad (3)$$

and

$$Y_{k(l)} = \sum_{m=1}^P \sum_{n=1}^R \left[W_{2,k(l,m,n)}^2 + W_{4,k(l,m,n)}^2 \right]. \quad (4)$$

Then the final decision variable of Eq(2) is obtained as $Z_{k(l)}^{DC} = X_{k(l)} - Y_{k(l)} = \sum_{m=1}^P \sum_{n=1}^R X_{k(l,m,n)} - \sum_{m=1}^P \sum_{n=1}^R Y_{k(l,m,n)}$, where $X_{k(l)}$ obeys a noncentral chi-square

Probability Density Function (PDF) with $2P \cdot R$ degrees of freedom and its noncentrality parameter λ_x is either $\frac{4N}{P} \left(\frac{E_c}{I_0} \right)'$, when the desired signal is deemed to be present ($x = 1$) or $\frac{4}{NP} \left(\frac{E_c}{I_0} \right)'$, when it is deemed to be absent ($x = 0$) [10]. The effects of both timing errors and the total frequency mismatches are encapsulated by the definition of $(E_c/I_0)'$. In the spirit of [2], $(E_c/I_0)'$ is defined as $(E_c/I_0)' = (E_c/I_0) \cdot \text{sinc}^2\left(\frac{\tau}{T_c}\right) \cdot \text{sinc}^2(N\Delta f_t T_c)$, where the second term of the definition is the square of the autocorrelation function imposed on the timing error, τ , the third term of the definition is the signal energy reduction expressed as a function of the total frequency mismatch, Δf_t after the squaring operation and N represents the number of chips accumulated over the

duration of τ_D . Finally, $Y_{k(l)}$ is centrally chi-square distributed with $2P \cdot R$ degrees of freedom. It is also worth noting that the outputs of the squaring operation invoked for both the in-phase and the quadrature branches in Fig.1 are modelled as squares of Gaussian random variables, respectively. Accordingly, the decision variable $X_{k(l,m,n)}$ of each path obeys a non-central chi-square PDF with two degrees of freedom [5], whereas $Y_{k(l,m,n)}$ is centrally chi-square distributed with two degrees of freedom. These PDFs are given by [12] as follows:

$$f_{X_{k(l,m,n)}}(z|H_x) = \frac{1}{2} \cdot \exp\left[-\frac{(z + \lambda_x)}{2}\right] \cdot \mathcal{I}_0\left(\sqrt{z \cdot \lambda_x}\right), \quad (5)$$

and

$$f_{Y_{k(l,m,n)}}(z|H_x) = \frac{1}{2} \cdot \exp\left[-\frac{z}{2}\right], \quad (6)$$

respectively, where $z \geq 0$, $x = 0$ or 1 , $\mathcal{I}_0(\cdot)$ is the $zero^{th}$ -order modified Bessel function of the first kind. Let us now express the PDF of the desired user's signal at the output of the acquisition scheme conditioned on the presence of the desired signal in $f_{X_{k(l,m,n)}}(z|H_x)$, when communicating over an uncorrelated Rayleigh channel. In this scenario E_c is multiplied by the square of the Rayleigh-distributed fading amplitude, β , which has a chi-square distribution with two degrees of freedom: $f(\beta) = \frac{e^{-\beta/\sigma^2}}{\sigma^2}$, where σ^2 is the variance of the constituent Gaussian distribution. Then the average pilot signal energy \bar{E}_c per PN code chip can be expressed as $\bar{E}_c = \beta E_c = \sigma^2 E_c$ [2]. Therefore first the PDF $f_{Z_{k(l,m,n)}}(z|H_x, \beta)$ corresponding to β conditioned on the hypothesis of the desired signal being transmitted over an AWGN channel having this specific SINR is weighted by the probability of occurrence $f(\beta)$ of encountering β , as quantified by the PDF. The resultant product is then averaged over its legitimate range of $-\infty \sim \infty$, yielding:

$$f_{X_{k(l,m,n)}}(z|H_x) = \int_{-\infty}^{\infty} f(\beta) \cdot f_{X_{k(l,m,n)}}(z|H_x, \beta) d\beta \quad (7)$$

$$= \int_0^{\infty} \left(\frac{e^{-\beta/\sigma^2}}{\sigma^2} \right) \cdot \frac{\exp[-(z + \beta\lambda_x)/2]}{2} \quad (8)$$

$$\cdot \mathcal{I}_0\left(\sqrt{\beta\lambda_x z}\right) d\beta = \frac{\exp[-z/(2 + \lambda_x\sigma^2)]}{(2 + \lambda_x\sigma^2)} \quad (9)$$

$$\equiv \frac{\exp[-z/(2 + \bar{\lambda}_x)]}{(2 + \bar{\lambda}_x)}, \quad (10)$$

where the corresponding noncentrality parameter of $\bar{\lambda}_x \equiv \lambda_x\sigma^2$ is either $\frac{4N}{P} \left(\frac{E_c}{I_0} \right)'$ when the desired signal is deemed to be present ($x = 1$) or $\frac{4}{NP} \left(\frac{E_c}{I_0} \right)'$ when it is deemed to be absent ($x = 0$). Similarly to the definition of $(E_c/I_0)'$, $(E_c/I_0)'$ is defined as $(E_c/I_0)' = (E_c/I_0) \cdot \text{sinc}^2\left(\frac{\tau}{T_c}\right) \cdot \text{sinc}^2(N\Delta f_t T_c)$. For notational convenience we also define a new biased noncentrality parameter $\mu_x = (2 + \bar{\lambda}_x)$. Further details on the related calculations are found in [2],[10]. Finally, we arrive at the PDF of $X_{k(l,m,n)}$ conditioned on the presence of the desired signal in the form of:

$$f_{X_{k(l,m,n)}}(z|H_x) = \frac{1}{\mu_x} e^{-z/\mu_x}. \quad (11)$$

The decision variables, $X_{k(l)}$ and $Y_{k(l)}$ are constituted by the sum of $P \cdot R$ number of independent variables ($X_{k(l)} = \sum_{m=1}^P \sum_{n=1}^R X_{k(l,m,n)}$ and $Y_{k(l)} = \sum_{m=1}^P \sum_{n=1}^R Y_{k(l,m,n)}$), each of which has a PDF given by Eq(11) or Eq(6), respectively. Both decision variables constitute independent Gamma variables, as mentioned in [2], leading to:

$$f_{X_{k(l)}}(z|H_x) = \frac{z^{(P \cdot R - 1)} e^{-z/\mu_x}}{\Gamma(P \cdot R) \cdot \mu_x^{P \cdot R}}, \quad (12)$$

$$f_{Y_{k(l)}}(z|H_x) = \frac{z^{(P \cdot R - 1)} e^{-z/2}}{\Gamma(P \cdot R) \cdot 2^{P \cdot R}}, \quad (13)$$

where we have $X_{tot} \sim g(P \cdot R, \mu_x)$ and $Y_{tot} \sim g(P \cdot R, 2)$ and $\Gamma(\cdot)$ is the Gamma function. This short-hand of $g(\cdot, \cdot)$ indicates that both X_{tot} and Y_{tot} follow a Gamma distribution having the shape parameter of $P \cdot R$ and a scale parameter of either μ_x or 2, respectively, as outlined in [18]. Then, the PDF of $Z_{k(l)}^{DC} = X_{k(l)} - Y_{k(l)}$ can be computed by straightforward convolution of the PDFs of both $X_{k(l)}$ and $Y_{k(l)}$, which results in the PDF of the difference between two independent Gamma variables. The convolution of the PDFs $f_{X_{k(l)}}$ and $f_{Y_{k(l)}}$ derived for calculating the PDF of $Z_{k(l)}^{DC}$ conditioned on the desired signal being present or absent is formulated as [18]:

$$f_{Z_{k(l)}^{DC}}(z|H_x) = \int_{-\infty}^{\infty} f_{X_{k(l)}}(\xi) \cdot f_{Y_{k(l)}}(\xi - z) d\xi \quad (14)$$

$$= \left(\frac{(1 - c^2)^{a + \frac{1}{2}} \cdot |z|^a}{\sqrt{\pi} \cdot 2^a \cdot b^{a+1} \cdot \Gamma(a + \frac{1}{2})} \right) \cdot \exp\left(-\frac{c}{b}z\right) \cdot K_a\left(\frac{|z|}{b}\right), z \neq 0, \quad (15)$$

where $a \equiv P \cdot R - 0.5$, $b \equiv (4\mu_x)/(\mu_x + 2)$ and $c \equiv -(\mu_x - 2)/(\mu_x + 2)$ as well as $K_a(\cdot)$ is the modified Bessel function of the second kind and of order a . We note furthermore that $K_a(\cdot)$ is undefined, when the argument is equal to zero. However, this fact has a negligible impact on calculating the probability of correct detection and false alarm. The probability of correct detection for the l^{th} path according to $x = 1$, is expressed as [18]:

$$P_{D(l)}^{DC} = \int_{\theta}^{\infty} f_{Z_{k(l)}^{DC}}(z|H_1) dz, \theta \neq 0, \quad (16)$$

where θ is a threshold value. Finally, the false alarm probability in the context of a H_0 hypothesis is expressed as

$$P_F^{DC} = \int_{\theta}^{\infty} f_{Z_{k(l)}^{DC}}(z|H_0) dz, \theta \neq 0. \quad (17)$$

B. Correct Detection and False Alarm Probability of the Non-coherent Code Acquisition Scheme

For comparison, the NC counterpart of the previously described DC scheme is characterised here, where the final decision variable of the l^{th} path is given by [10]

$$Z_{k(l)}^{NC} = \sum_{m=1}^P \sum_{n=1}^R \left\| \frac{1}{\sqrt{2}} \cdot \left(\sqrt{\frac{4E_c}{NI_0P}} \cdot S_{k(l,m,n)} + I_{k(l,m,n)} \right) \right\|^2, \quad (18)$$

where $\|\cdot\|^2$ represents the Euclidian norm of the complex-valued argument and the factor of $1/\sqrt{2}$ is employed to

normalise the noise variance. The NC decision variable $Z_{k(l)}^{NC}$ has exactly the same statistical behaviour as $X_{k(l)}$ described in Section A and hence its derivation follows the same procedure as that of $f_{X_{k(l)}}(z|H_x)$ outlined in Section A. $S_{k(l,m,n)}$ becomes deterministic [10], while $I_{k(l,m,n)}$ is the complex-valued AWGN having zero means and variances of $\sigma^2=2$ for both their real and imaginary parts. Finally, the probability of correct detection corresponding to $x = 1$ for the l^{th} path is obtained as

$$P_{D(l)}^{NC} = \exp\left(-\frac{\theta}{\mu_1}\right) \cdot \sum_{k=0}^{P \cdot R - 1} \frac{(\theta/\mu_1)^k}{k!}, \quad (19)$$

while the false alarm probability in the context of a H_0 hypothesis is expressed as

$$P_F^{NC} = \exp\left(-\frac{\theta}{\mu_0}\right) \cdot \sum_{k=0}^{P \cdot R - 1} \frac{(\theta/\mu_0)^k}{k!}, \quad (20)$$

where μ_x is again set to be $(2 + \bar{\lambda}_x)$ and $\bar{\lambda}_x$ is either $\frac{2N}{P} \left(\frac{E_c}{I_0}\right)'$ for the hypothesis of the desired signal being present ($x = 1$) or $\frac{2}{NP} \left(\frac{E_c}{I_0}\right)'$ for it being absent ($x = 0$).

C. Mean Acquisition Time Analysis

In [2],[16] explicit MAT formulas were provided for a single-antenna-aided serial search based code acquisition system. There is no distinction between a single-antenna-aided scheme and a multiple-antenna assisted one in terms of analysing their MAT performance, except for deriving their correct detection and the false alarm probability based upon using transmit/receive antennas. We will commence our discourse by analysing the MAT performance of both DC and NC acquisition schemes, employed in SDSS and DDSS. We assume that in each chip duration T_c , α number of timing hypotheses are tested, which are spaced by T_c/α . Hence the total uncertainty region is increased by a factor of α . Moreover, when the L multi-path signals arrive with time delays τ_l having a tap spacing of one chip-duration, the relative frequency of the signal being present is increased L -fold. The required transfer functions [2],[16], are defined as follows. The entire successful detection function $H_D(z)$ encompasses all the branches of a state diagram [2],[16], which lead to successful detection. Furthermore, $H_0(z)$ indicates the absence of the desired user's signal at the output of the acquisition scheme, while $H_M(z)$ represents the overall miss probability of a search run carried out across the entire uncertainty region. The related processes are detailed for SDSS in [2] and for DDSS in [16]. Then, it may be shown that the generalised expression derived for computing the MAT of the serial search based code acquisition scheme is given by [2],[16]:

$$E[T_{ACQ}] = \frac{1}{H_D(1)} [H_D'(1) + H_M'(1) + \{(\nu - 2\alpha L) \left[1 - \frac{H_D(1)}{2}\right] + \frac{1}{2} H_D(1)\} H_0'(1)] \cdot \tau_D, \quad (21)$$

where $H_x'(z)|_{x=D, M \text{ or } 0}$ is a derivative of $H_x(z)|_{x=D, M \text{ or } 0}$ and τ_D denotes either the dwell time³ for the SDSS scenario

³The dwell time is defined as the time-interval, during which the acquisition scheme 'dwells' in the interval $\tau_D \equiv NT_c$ accumulating the correlation contributions, which quantify the similarity of the locally stored and received spreading sequence.

or the dwell time of the search mode for the DDSS case. If the total number of states ν is significantly higher than the number of H_D states [5], the exact MAT formula of Eq(21) can be simplified as follows:

$$E[T_{ACQ}] \approx \frac{(1 + H_M(1)) \cdot H_0'(1)}{2 \cdot (1 - H_M(1))} \cdot (\nu \cdot \tau_D). \quad (22)$$

In order to simplify our numerical performance analysis, we adopted the approximation of the exact MAT expression proposed in [5], as indicated in Eq(22). Since each resolvable path contributes two hypotheses and because the average correct detection probability associated with these two hypotheses is the same, the overall miss probabilities of both the SDSS and the DDSS schemes may be expressed as

$$H_M(1) = \prod_{l=1}^L \prod_{\zeta=1}^{\alpha} (1 - P_{D(l,\zeta)})^2 \quad (23)$$

and

$$H_M(1) = \prod_{l=1}^L \prod_{\zeta=1}^{\alpha} [(1 - P_{D1(l,\zeta)}) + P_{D1(l,\zeta)} \cdot (1 - P_{D2(l,\zeta)})]^2, \quad (24)$$

respectively, where $P_{D(l,\zeta)}$ represents the correct detection probability of the SDSS scheme and $P_{Dx(l,\zeta)}|_{x=1, \text{ or } 2}$ are the correct detection probability of both the search and the verification modes of the DDSS arrangements, respectively. Both $P_{D(l,\zeta)}$ and $P_{Dx(l,\zeta)}$ are given by either Eq(16) or Eq(19). The $H_0'(1)$ values of the SDSS and DDSS schemes are expressed as

$$H_0'(1) = 1 + K \cdot P_F \quad (25)$$

and

$$H_0'(1) = 1 + \epsilon \cdot P_{F1} + K \cdot P_{F1} \cdot P_{F2}, \quad (26)$$

respectively, where K denotes the false locking penalty factor expressed in terms of the number of chip intervals required by an auxiliary device for recognising that the code-tracking loop is still unlocked and ϵ represents the ratio defined as the dwell time for the verification mode over that for the search mode. Furthermore, P_F is the false alarm probability of the SDSS scheme and $P_{Fx}|_{x=1, \text{ or } 2}$ represent the false alarm probability of both the search and the verification mode of the DDSS scheme, respectively. Similarly, both P_F and P_{Fx} are given by either Eq(17) or Eq(20).

IV. NUMERICAL SYSTEM PERFORMANCE RESULTS

In this section we will characterise the MAT performance of MIMO-aided DS-CDMA systems. The associated system parameters are summarised in Table I. In Table II we outlined the maximum SINR degradation imposed by both the Doppler shift and the clock-drift-induced frequency mismatch between the transmitter and receiver in conjunction with a coherent integration interval of N chip durations, where both represent the total frequency mismatch. These values were calculated by using Eq(3.7) on page 47 of [2] provided for determining the performance degradation owing to the total frequency mismatch imposed both by the Doppler shift and by the clock drift. The length of the PN sequence in our system

TABLE I
SYSTEM PARAMETERS

Bandwidth	1.2288MHz	
Carrier frequency	1.9GHz	
Spreading factor	128	
Diversity:	Transmit	1,2,4
	Receive	1,2,4
Clock drift	1000Hz	
Mobile speed	160km/h	
Number of chip (SDSS)	256 chips	
Number of chip (DDSS)	64 and 256 chips	
Total uncertainty region	512	
False locking penalty factor	1000	
Number of paths	single and three path(s)	

TABLE II
MAXIMUM SINR DEGRADATION INFLICTED BY BOTH THE DOPPLER SHIFT AND THE CLOCK DRIFT IN CONJUNCTION WITH THE COHERENT INTEGRATION INTERVAL OF N CHIP DURATIONS AT A CARRIER FREQUENCY OF 1.9GHZ

N (Chips)	64	128	256	384	512
Degradation [dB]	0.061	0.2449	0.9969	2.3144	4.3213

was assumed to be $256 \cdot T_c$, where the chip-duration is $T_c = 1/1.2288 \mu\text{s}$. When adopting the above-mentioned FPC scheme of [10] for analysing SDSS, based on our results not included here owing to lack of space, it was found to be sufficient to integrate the detector output seen in Fig.1 over $N = 256$ chips. In the DDSS case the number of chips, over which the accumulator in Fig.1 sums the envelope detector's output, is assumed to be 64 for the search mode and 256 for the verification mode in all the different transmit/receive antenna scenarios. These values were also calculated by employing Eq(3.7) on page 47 of [2]. The spreading factor of the Walsh code to be acquired was selected to be 128. The clock-drift-induced frequency mismatch was assumed to be 1000Hz [2], while the carrier frequency was 1.9GHz. As an example of a high mobile speed, it is reasonable to postulate 160 km/h. We also assumed that the sampling inaccuracy caused by having a finite, rather than infinitesimally small search step size of $\Delta = T_c/2$ was -0.91dB ⁴, where $\Delta = T_c/2$ represents a typical value for the search step size [2]. The total uncertainty region was assumed to entail 512 hypotheses. In the spirit of [16], the false locking penalty factor was assumed to be 1000 chip-durations. Finally, it is assumed that both single-path and multi-path scenarios are considered. Three paths arriving with a relative time delay of one chip and having a magnitude difference of 3dB, respectively were assumed. In all the remaining figures we assumed an operation in the range of 'finger locking', which may be considered to be the range between $E_c/I_0 = -17$ and -13dB , as suggested in [19],[20]. All the performance curves have been generated at the threshold value of $E_c/I_0 = -16\text{dB}$, which was considered as the minimum value required for finger locking.

Fig.3 illustrates the achievable MAT versus SINR per chip

⁴A half-chip-duration timing error imposed on the single hypothesis test per chip is capable of causing an SINR loss of several dBs, when considering the achievable MAT performance, which was deemed excessive. Hence we opted for testing two hypotheses per chip, which reduced the corresponding SINR loss to 0.91dB [2].

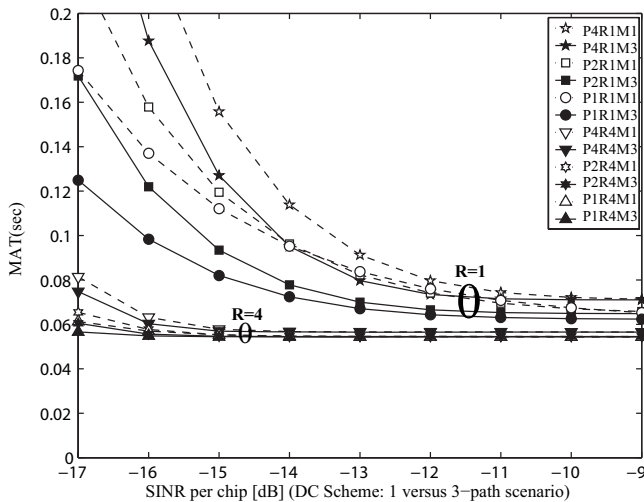


Fig. 3. MAT versus SINR per chip performance of the DC code acquisition system for SDSS parameterised with both the number of transmit and receive antennas.

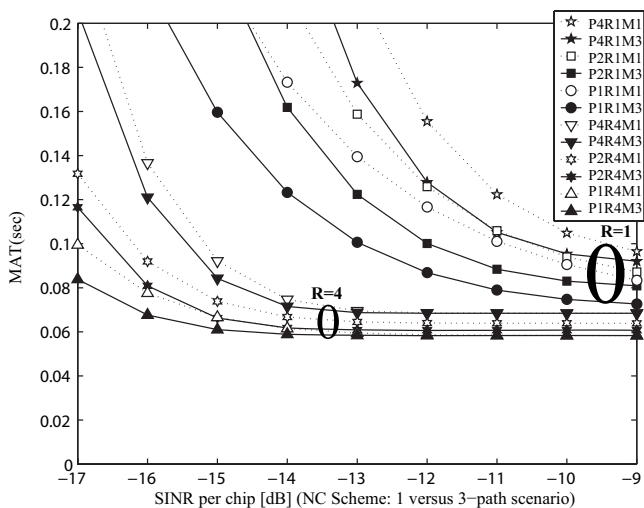


Fig. 4. MAT versus SINR per chip performance of the NC code acquisition system for SDSS parameterised with both the number of transmit and receive antennas.

performance of the DC SDSS code acquisition scheme as a function of the number of transmit antennas for $P = 1, 2$ as well as 4 and that of the number of receive antennas for $R = 1$ and 4. In the results of Figs.3 to 6, the solid lines indicate the scenario of receiving three paths (denoted as $M3$ in Figs.3 to 6), whereas the dashed lines represent a single-path scenario (denoted as $M1$ in Figs.3 to 6). For the sake of compact notation, the scenario of using $P = x$, $R = y$ and $M = z$ is denoted as $PxRyMz$ in Figs.3 to 6. Observe in Fig.3 that somewhat surprisingly, as the number of transmit antennas is decreased, we experience an improved MAT performance for both the single-path and multi-path scenarios. The main reasons for the performance trends will be further justified by information theoretic considerations in the NC MIMO-aided scenarios at the end of the section. On the other hand, the MAT performance of the multi-path scenario became better than that of the single-path one, since the number of the states with the signal being present was increased by a factor of three. In the

TABLE III

THE MAT PERFORMANCE RATIO BETWEEN NC SDSS AND DC SDSS AS WELL AS NC DDSS AND DC DDSS AT $E_c/I_0 = -15$ DECIBEL

	DC SDSS/ NC SDSS	DC DDSS/ NC DDSS
P4	3.2443	2.5727
P2	2.5	2.0704
P1	2.0208	1.7615

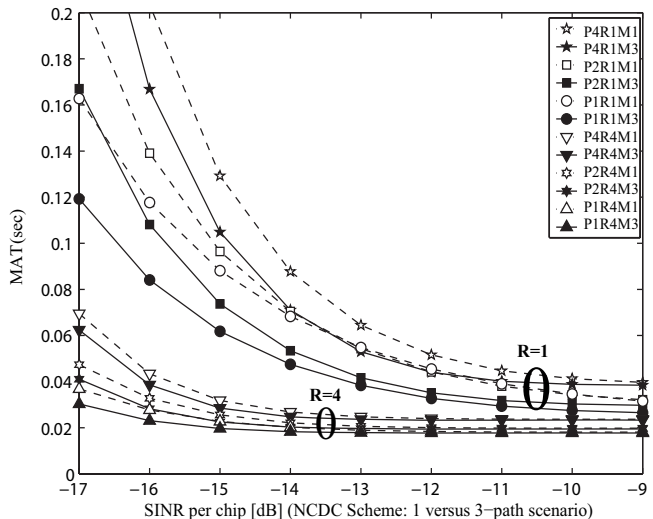


Fig. 5. MAT versus SINR per chip performance for a DDSS system constituted by both the NC code acquisition system in the search mode and the DC code acquisition system in the verification mode parameterised with both the number of transmit and receive antennas.

case of $R = 4$ receivers the performance improvements due to having multiple paths became marginal, because the receive diversity gain was already sufficiently high for approaching a Gaussian MAT-performance. A useful transmit diversity gain was achievable only for the $P = 2$ and $R = 1$ scenario, and this was limited to the specific SINR range of -10 to -14 dB in the single-path scenario. For comparison, Fig.4 characterises the MAT versus SINR per chip performance of the NC SDSS code acquisition system as a function of the number of transmit antennas for $P = 1, 2$ as well as 4 and that of the number of receive antennas for $R = 1$ and 4. Similarly, as the number of transmit antennas is decreased, all the curves illustrate an improved MAT performance. In particular, the MAT performance of the DC scheme clearly shows a better performance in comparison to the NC arrangement, since the DC scheme has a performance gain of approximately 3 dB in comparison to the NC scheme. Furthermore, the DC scheme is more efficient in terms of reducing the effects of both the AWGN and the interference, than the NC one in the low SINR range [9] ⁵. Hence, the DC scheme suffers from a less severe MAT performance degradation owing to employing multiple transmit antennas in comparison to its NC counterpart.

Fig.5 characterises the MAT versus SINR per chip performance of a DDSS system. More specifically, both the NC code acquisition-aided system of Fig.1 used in the search mode and

⁵In the low SINR region, the false alarm probabilities of the DC and NC schemes differ by a factor of two. This fact leads to the superiority of the DC scheme over the NC arrangement.

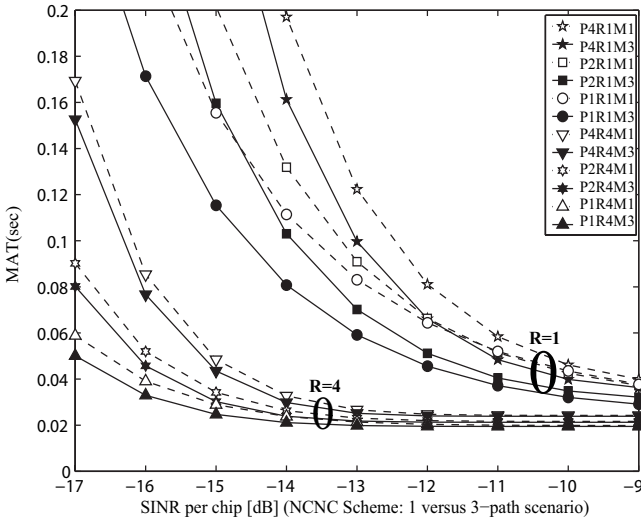


Fig. 6. MAT versus SINR per chip performance of the NC code acquisition system for DDSS parameterised with both the number of transmit and receive antennas.

the DC code acquisition assisted scheme of Fig.1 employed in the verification mode are characterised. Explicitly, their performance is quantified as a function of the number of transmit antennas for $P = 1, 2$ as well as 4 and the number of receive antennas for $R = 1$ and 4 (denoted as *NCDC* for $P = 1, 2$ and 4 in the verification mode of both the DC and NC in Fig.5). By contrast, Fig.6 characterises the MAT versus SINR per chip performance of a DDSS system employing the NC code acquisition-aided scheme of Fig.1 in both its search mode and verification mode (denoted as *NCNC* in Fig.6). The results seen in Fig.5 suggest that the overall performance improvement of the DDSS system employing the DC scheme of Fig.1 in its verification mode is significantly higher than that of the DDSS system using the NC scheme of Fig.1, as seen in Fig.6. Similarly to the results of the SDSS scenario in both Figs.3 and 4, the MAT performance degradation becomes more drastic in Figs.5 and 6, when the number of transmit antennas is increased, as observed for the DC and NC schemes, respectively. Nonetheless, as expected, the overall performance of DDSS remains substantially higher than that of SDSS. In the case of DDSS, the performance improvement obtained for the three-path scenario is less than that of SDSS. It is worth mentioning that although not explicitly shown in Figs.3 to 6 for avoiding obfuscating details, the MAT operating range of $R = 2$ receive antennas was found to be between that corresponding to the $R = 1$ and $R = 4$ receive antenna scenario. Observe in Figs.3 to 6 that the discrepancy between the MAT of SDSS and that of DDSS becomes more drastic, when the number of transmit antennas increases. In the multi-path scenarios all the results fail to show a transmit diversity gain, since the third-order receive diversity provided by the three paths approaches a Gaussian performance. Table III summarises the performance improvements inferred from Figs.3 to 6 for the DC code acquisition scheme over the NC arrangement in the case of experiencing a single path, when considering $P = 1, 2$ and 4 number of transmit antennas invoked in conjunction with $R = 1$ receive antenna. Observe in this table, that the performance improvements achieved by employing the DC SDSS and DDSS schemes becomes

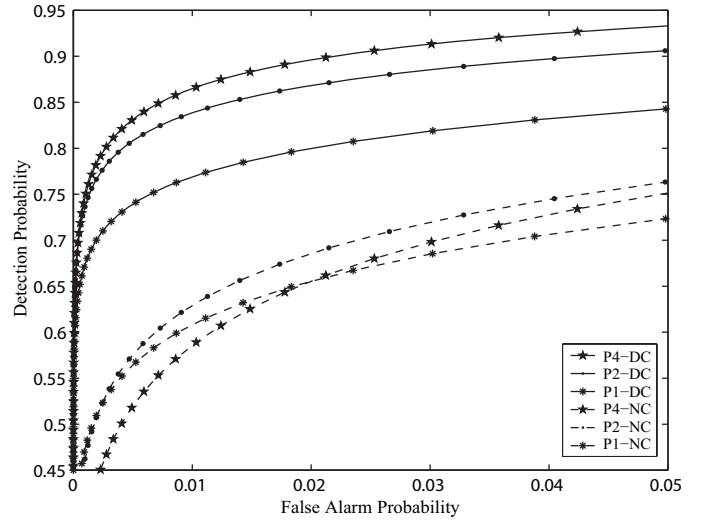


Fig. 7. Correct detection versus false alarm probability of $P=1, 2$ and 4 transmit antennas for both DC and NC code acquisition in the verification mode of our DDSS schemes at 2nd dwell.

significantly higher in the vicinity of $E_c/I_0 = -15$ dB, when the number of transmit antennas is increased.

Fig.7 illustrates the correct detection versus false alarm probability, parameterised by the number of transmit antennas for $P = 1, 2$ and 4 in the verification mode of both the DC and NC schemes at $E_c/I_0 = -13$ dB. In terms of the achievable MAT performance, the most efficient operational range of the false alarm probabilities for the verification mode and for the search mode is in the range of 10^{-3} to 10^{-4} . In this range the values of correct detection probability sharply decrease, as seen in Fig.7. The reason that the false alarm probability should be small is directly related to the value of the aforementioned false locking penalty associated with the false alarm event(s). A high value of the penalty factor leads to a further degraded MAT performance. Accordingly, a low false alarm probability results in the best possible MAT performance. Having a high correct detection probability would also improve the MAT, but finding the optimum of this probability may be challenging, whilst maintaining as low a false alarm probability as possible. Furthermore, observe in Fig.7 that the performance of $P = 4$ is the worst in the context of the NC DDSS scheme and $P = 1$ is the best, in particular at 10^{-3} and lower ranges of the false alarm probability. The DC scheme also exhibits similar trends for the DDSS scheme, although the degree of performance degradation is smaller than that of the NC scheme at E_c/I_0 values below those seen in Fig.7. More explicitly, the performance of the correct detection versus false alarm probability recorded for the DC scheme at $E_c/I_0 = -16$ dB is similar to that of the NC scheme at $E_c/I_0 = -13$ dB in Fig.7. Additionally, it is worth noting that the useful operational range of the false alarm probability for the search mode is 0.05 to 0.25 for values of $R = 1$ to 4. The correct detection probability increases rapidly over this range of the probability of false alarm.

The fact that multiple transmit antennas degrade the achievable MAT performance can be further explained as follows. A low level of per-branch received signal strength would lead to a low acquisition performance. In other words, a high diversity

order effectively results in an acquisition performance loss, as a consequence of the insufficiently high transmit signal strength per branch. In case of employing both multiple transmit and multiple receive antennas, similar trends are observable, although using two or four receive antennas has the potential of mitigating the associated acquisition performance degradation imposed by the low per-branch E_c/I_0 values associated with the employment of multiple transmitters. The main reasons for the above-mentioned performance trends may be further justified by information theoretic considerations in the NC MIMO-aided scenarios considered [21],[22].

The main reasons for the above-mentioned phenomenon are multifold:

1) In general, coherently detected space-time transmission schemes benefit from having explicit knowledge of the channel's impulse response, which is unavailable during the code-acquisition phase. Using a relatively low number of chips, over which integration or accumulation is carried out imposes further limits on the attainable benefits of MIMO schemes [21],[22].

2) Since no channel coding is used for the pilot signal, no time diversity gain associated with interleaving and channel coding can be achieved [23].

3) When the detection threshold θ_2 of Fig.2 is reduced, the resultant code phase estimate often cannot be confirmed by the verification stage of Fig.2 and hence the resultant false alarm probability is increased. At the same time, the correct detection probability is also increased. However, when aiming for the best achievable MAT performance, the detection threshold optimisation has to strike a balance between increasing the false alarm probability and the correct detection probability, because after a false alarm event the system may require a high number of chip-durations to return to its search mode.

4) The effect of using a fixed threshold pair θ_1 and θ_2 , which is optimised for a specific E_c/I_0 value, also limits the attainable MAT performance, since the acquisition threshold should be optimised and controlled as a function of the E_c/I_0 value encountered.

V. CONCLUSION

In this paper, we analysed the multiple antenna-aided transmit/receive diversity effects of the acquisition performance of both DC and NC code acquisition schemes in the CDMA DL. The probabilities of correct detection and false alarm have been derived analytically and numerical results have been provided in terms of the MAT performance. Our numerical results show that increasing the number of transmit antennas in a MIMO-aided CDMA system results in a MAT performance degradation, regardless whether single-path or multi-path scenarios are considered. This fact suggests that employing a single transmit antenna might be recommended during code acquisition for optimising the achievable MAT performance. Our findings were further corroborated by information theoretic considerations in the NC MIMO-aided scenarios.

ACKNOWLEDGEMENT

The financial support of the Ministry of Information and Communication (MIC), Republic of Korea, of the EPSRC,

UK and of the EU is gratefully acknowledged.

REFERENCES

- [1] D. Gesbert, M. Shafi, D. S. Shiu, P. J. Smith, and A. Naguib, "From theory to practice: an overview of MIMO space-time coded wireless systems," *IEEE J. Select. Areas Commun.*, vol. 21, no. 3, pp. 281–302, 2003.
- [2] A. J. Viterbi, *CDMA: Principles of Spread Spectrum Communication*, chapter 3. Addison-Wesley, 1995.
- [3] M. K. Simon, J. K. Omura, R. A. Scholtz, and B. K. Levitt, *Spread Spectrum Communications Handbook*, part 4, chapter 1. McGraw-Hill Professional, 2001.
- [4] B.-G. Lee and B.-H. Kim, *Scrambling Techniques For CDMA Communications*, chapters 3 and 4. Kluwer Academic Publishers, 2001.
- [5] L.-L. Yang and L. Hanzo, "Serial acquisition of DS-SS signals in multipath fading mobile channels," *IEEE Trans. Veh. Technol.*, vol. 50, no. 2, pp. 617–628, 2001.
- [6] W. Suwansantisuk, M. Z. Win, and L. A. Shepp, "On the performance of wide-bandwidth signal acquisition in dense multipath channels," *IEEE Trans. Veh. Technol.*, vol. 54, no. 5, pp. 1584–1594, 2005.
- [7] Y. Ikai, M. Katayama, T. Yamazato, and A. Ogawa, "A new acquisition scheme of a DS/SS signal with transmit and receive antenna diversity," in *Proc. IEEE ICC*, vol. 2, 1999, pp. 1256–1261.
- [8] S. H. Won and Y. J. Kim, "Performance analysis of multi-path searcher for mobile station in W-CDMA system employing transmit diversity," *Electron. Lett.*, vol. 39, no. 1, pp. 137–139, 2003.
- [9] M. H. Zarrabizadeh and E. S. Sousa, "A differentially coherent PN code acquisition receiver for CDMA systems," *IEEE Trans. Commun.*, vol. 45, no. 11, pp. 1456–1465, 1997.
- [10] J.-C. Lin, "Differentially coherent PN code acquisition with full-period correlation in chip-synchronous DS/SS receivers," *IEEE Trans. Commun.*, vol. 50, no. 5, pp. 698–702, 2002.
- [11] O. S. Shin and K. B. Lee, "Differentially coherent combining for double-dwell code acquisition in DS-SS systems," *IEEE Trans. Commun.*, vol. 51, no. 7, pp. 1046–1050, 2003.
- [12] J. G. Proakis, *Digital Communications, 4th ed*, chapter 2. McGraw-Hill, 2001.
- [13] G. E. Corazza, C. Caini, A. Vanelli-Coralli, and A. Polydoros, "DS-SS code acquisition in the presence of correlated fading—part I: theoretical aspects," *IEEE Trans. Commun.*, vol. 52, no. 7, pp. 1160–1168, 2004.
- [14] G. E. Corazza, C. Caini, A. Vanelli-Coralli, and A. Polydoros, "DS-SS code acquisition in the presence of correlated fading—part II: application to cellular networks," *IEEE Trans. Commun.*, vol. 52, no. 8, pp. 1397–1407, 2004.
- [15] R. N. McDonough and A. D. Whalen, *Detection of Signals in Noise, 2nd ed*, chapter 5. Academic Press, Inc., 1995.
- [16] H. R. Park, "Performance analysis of a double-dwell serial search technique for cellular CDMA networks in the case of multiple pilot signals," *IEEE Trans. Veh. Technol.*, vol. 48, no. 6, pp. 1819–1830, 1999.
- [17] W. Suwansantisuk and M. Z. Win, "Multipath aided rapid acquisition: optimal search strategies," *IEEE Trans. Inform. Theory*, vol. 53, no. 1, pp. 174–193, 2007.
- [18] H. Holm and M.-S. Alouini, "Sum and difference of two squared correlated Nakagami variates in connection with the McKay distribution," *IEEE Trans. Commun.*, vol. 52, no.8, pp. 1367–1376, 2004.
- [19] C. Noblet, M. Fadridis, and R. Owen, "Downlink transmit power issues in a WCDMA cellular system," 3G Mobile Communication Technologies, 2002 Conference Publication No.489, 8-10 May 2002, pp. 244–249.
- [20] J. S. Lee and L. E. Miller, *CDMA Systems Engineering Handbook*, chapter 11, CDMA Optimization Issues. Artech House Publishers, 1998.
- [21] T. L. Marzetta and B. M. Hochwald, "Capacity of a mobile multiple-antenna communication link in Rayleigh flat fading," *IEEE Trans. Inform. Theory*, vol. 45, no.1, pp. 139–157, 1999.
- [22] L. Zheng and D. N. C. Tse, "Communication on the Grassmann manifold: a geometric approach to the noncoherent multiple-antenna channel," *IEEE Trans. Inform. Theory*, vol. 48, no. 2, pp. 359–383, 2002.
- [23] H.-F. Lu and P. V. Kumar, "Rate-diversity tradeoff of space-time codes with fixed alphabet and optimal constructions for PSK modulation," *IEEE Trans. Inform. Theory*, vol. 49, no. 10, pp. 2747–2751, 2003.



SeungHwan Won (M'04) received the B.S. and M.S. degrees in Radio Science and Engineering from Korea University, Seoul, Republic of Korea, in 1999 and 2001, respectively. He was a research engineer in Mobile Communication Technology Research Lab, LG Electronics R&D, from January 2001 to September 2004. He was the recipient of the 2004 state scholarship of the Information and Telecommunication National Scholarship Program, Ministry of Information and Communication (MIC), Republic of Korea. Since October 2004, he has

been working towards the Ph.D. degree in the Communications Research Group, School of Electronics and Computer Science at the University of Southampton, UK. His major research interests include initial synchronization in non-coherent MIMO aided single- and multi-carrier CDMA, DS-UWB and OFDMA as well as in iterative synchronization schemes designed for MIMO aided single- and multi-carrier transmission systems.



Lajos Hanzo, Fellow of the Royal Academy of Engineering, received his first-class degree in electronics in 1976 and his doctorate in 1983. In 2004 he was awarded the Doctor of Sciences (DSc) degree by the University of Southampton, UK. During his career in telecommunications he has held various research and academic posts in Hungary, Germany and the UK. Since 1986 he has been with the Department of Electronics and Computer Science, University of Southampton, UK, where he holds the chair in telecommunications. He co-authored 15

John Wiley and IEEE Press books totalling 10 000 pages on mobile radio communications, published about 700 research papers, organised and chaired conference conferences, presented various keynote and overview lectures and has been awarded a number of distinctions. Currently he heads an academic research team, working on a range of research projects in the field of wireless multimedia communications sponsored by industry, the Engineering and Physical Sciences Research Council (EPSRC) UK, the European IST Programme and the Mobile Virtual Centre of Excellence (VCE), UK. He is an enthusiastic supporter of industrial and academic liaison and he offers a range of industrial courses. Lajos is also an IEEE Distinguished Lecturer of both the Communications as well as the Vehicular Technology Society, a Fellow of both the IEEE and the IEE. He is an editorial board member of the Proceedings of the IEEE, a Governor of the IEEE VT Society, and the EIC of the IEEE Press. For further information on research in progress and associated publications please refer to <http://www-mobile.ecs.soton.ac.uk>